# Size Dependence of Atomically Precise Gold Nanoclusters in Chemoselective Hydrogenation and Active Site Structure

Gao Li,[†] De-en Jiang,[‡] Santosh Kumar,[†] Yuxiang Chen,[†] and Rongchao Jin[*,†]

[†]Department of Chemistry, Carnegie Mellon University, Pittsburgh, Pennsylvania 15213, United States
[‡]Chemical Sciences Division, Oak Ridge National Laboratory, Oak Ridge, Tennessee 37831, United States

S *Supporting Information*

ABSTRACT: We investigate the catalytic properties of water-soluble $Au_n(SG)_m$ nanocluster catalysts (H-SG = glutathione) of different sizes, including $Au_{15}(SG)_{13}$, $Au_{18}(SG)_{14}$, $Au_{25}(SG)_{18}$, $Au_{38}(SG)_{24}$, and captopril-capped $Au_{25}(Capt)_{18}$ nanoclusters. These $Au_n(SR)_m$ nanoclusters (SR represents thiolate generally) are used as homogeneous catalysts (i.e., without supports) in the chemoselective hydrogenation of 4-nitrobenzaldehyde ($4-NO_2PhCHO$) to 4-nitrobenzyl alcohol ($4-NO_2PhCH_2OH$) with ~100% selectivity in water using H_2 gas (20 bar) as the hydrogen source. These nanocluster catalysts, except $Au_{18}(SG)_{14}$, remain intact after the catalytic reaction, evidenced by UV−vis spectra, which are characteristic of nanoclusters of each size and thus serve as spectroscopic "fingerprints". We observe a drastic size dependence and steric effect of protecting ligands on the gold nanocluster catalysts in the hydrogenation reaction. Density functional theory (DFT) modeling of the 4-nitrobenzaldehyde adsorption shows that both the -CHO and -NO$_2$ groups closely interact with the S-Au-S staples on the gold nanocluster surface. The adsorptions of the 4-nitrobenzaldehyde molecule on the four different sized $Au_n(SR)_m$ nanoclusters are moderately strong and similar in strength. The DFT results suggest that the catalytic activity of the $Au_n(SR)_m$ nanoclusters is primarily determined by the surface area of the Au nanocluster, consistent with the observed trend of the conversion of 4-nitrobenzaldehyde versus the cluster size. Overall, this work offers molecular insight into the hydrogenation of 4-nitrobenzaldehyde and the catalytically active site structure on gold nanocluster catalysts.
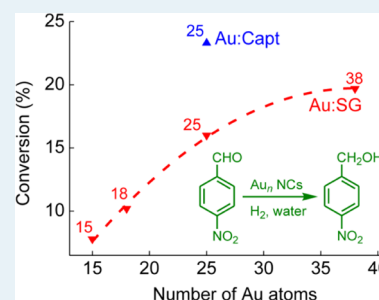
KEYWORDS: *Au nanocluster, water-soluble, hydrogenation, chemoselective, size dependence*

■ INTRODUCTION

Well-defined gold nanoclusters with ~10 to a few hundred gold atoms (i.e., core size ranging from 1 to 2 nm) constitute a new and promising class of material and are attracting significant research interest.[1−8] These atomically precise gold nanoclusters with an organic shell (e.g., thiolate), formulated as $Au_n(SR)_m$ (n and m represent the numbers of gold atoms and thiolate molecules, respectively), have been applied in a range of catalytic reactions, such as selective oxidation and hydrogenation as well as carbon−carbon cross-coupling reactions.[9−12] It is well-known that the catalytic properties of nanocatalysts are largely affected by the surface area of the particle. Unlike conventional gold nanocatalysts (e.g., naked nanoparticles) whose exact surface structures are largely unknown, more and more atomically precise nanoclusters are being crystallographically characterized.[2] The structures of $Au_n(SR)_m$ generally exhibit a gold kernel protected by staplelike surface motifs, and the surface area of these well-defined gold nanoclusters is mainly determined by the staple shell comprising both surface gold atoms and the protecting ligands. Gold nanoclusters have unique Au core packing modes and different protecting staple motifs; for example, the $Au_{25}(SR)_{18}$ nanocluster[13] comprises an Au_{13} icosahedral core (or kernel) and a staple shell comprising six $Au_2(SR)_3$ (-SR-Au-SR-Au-SR-) dimeric staples (Scheme 1d), and the $Au_{38}(SR)_{24}$ nanocluster[14]

consists of a biicosahedral Au_{23} core and six dimeric $Au_2(SR)_3$ and three monomeric $Au(SR)_2$ (-SR-Au-SR-) staples (Scheme 1f). These well-defined gold nanoclusters with known crystal structures can be employed as model catalysts to investigate the correlation between the catalytic performance and the gold nanocatalyst structure.[9] The unique cluster structures provide an exciting opportunity to gain insight into the mechanism of nanocatalysis.

In recent studies, conventional gold nanoparticles (polydispersed ones, usually between 2 and 20 nm) have been widely applied in the selective hydrogenation reactions.[15−20] For example, Corma and co-workers studied hydrogenation of nitroaromatics with an aldehyde substituent by H_2 and found that the Au/TiO_2 catalyst can selectively reduce nitro compounds to amines instead of aldehyde to alcohol.[21] Ultrasmall gold nanoparticles (1−2 nm) also exhibit good catalytic activity in the hydrogenation processes.[22−26] In our recent work, we investigated the catalytic performance of the unsupported and oxide-supported $Au_n(SPh)_m$ nanoclusters (n = 25, 36, and 99, and m = 18, 24, and 42, respectively) in the chemoselective hydrogenation of the reactants with both nitro

Scheme 1. Molecular Structures of (a) Glutathione and (b) Captopril and Cluster Structures of (c) $Au_{15}(SR)_{13}$,[27] (d) $Au_{25}(SR)_{18}$,[13] (e) $Au_{18}(SR)_{14}$,[28] and (f) $Au_{38}(SR)_{24}$[14] Nanoclusters[a]
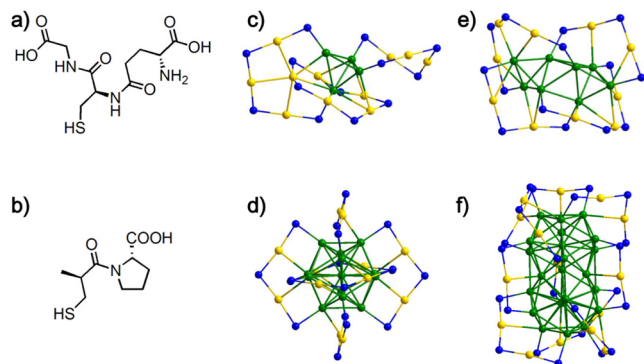
[a]Carbon and hydrogen atoms have been omitted for the sake of clarity. Color code: green for core Au, yellow for surface Au, and blue for S.

and aldehyde functional groups (e.g., nitrobenzaldehyde) to alcohols (e.g., nitrobenzyl alcohol) using H_2 as a hydrogen source.[25] Remarkably, a complete chemoselectivity for alcohol (~100%) was obtained, and oxide-supported $Au_n(SPh)_m$ nanoclusters offer a high level of conversion (80−99%) in water (solvent); however, the unsupported nanoclusters were less efficient and gave rise to only ~10% conversion of nitrobenzaldehyde in a homogeneous solution using a toluene/ethanol mixture as the solvent.[25] All of the works mentioned above mainly focus on the organic soluble $Au_n(SR)_m$ nanocluster catalysts supported on various oxides, but how the water-soluble $Au_n(SR)_m$ nanoclusters perform in aqueous-phase homogeneous catalysis remains unclear.

Herein, we are motivated to explore the catalytic activity of aqueous soluble $Au_n(SR)_m$ nanocluster catalysts as homogeneous catalysts for chemoselective hydrogenation of 4-nitrobenzaldehyde (4-NO_2PhCHO). The nanoclusters studied in this work include $Au_{15}(SG)_{13}$, $Au_{18}(SG)_{14}$, $Au_{25}(SG)_{18}$, $Au_{38}(SG)_{24}$, and $Au_{25}(Capt)_{18}$ nanoclusters, where SG and Capt stand for glutathione and captopril, respectively; note that the $Au_{25}(SG)_{18}$ nanocluster throughout this work is anionic {i.e., $[Au_{25}(SG)_{18}]^-$ in the native state}, whereas others are charge neutral. The reaction is conducted in water (the cheapest and environmentally friendly solvent) under relatively mild conditions (80 °C, 20 bar of H_2 gas). A complete chemoselectivity to the 4-nitrobenzyl alcohol (4-NO_2PhCH_2OH) product is obtained, and the catalytic activity exhibits a distinct size dependence on the gold core (from Au_{15} to Au_{38}, size range from ~0.8 to ~1.3 nm) and also a distinct ligand effect [i.e., glutathione vs captopril (Scheme 1a,b)]. Therefore, both the gold core size and the protecting organic ligands are important factors in the catalytic process. Further, the available nanocluster structures[13,14,27,28] (Scheme 1c−f) permit density functional theory (DFT) modeling, and insights into the reactant adsorption mode and catalytically active sites are obtained for the selective hydrogenation reaction.

■ **EXPERIMENTAL METHODS**

Synthesis of $Au_n(SG)_m$ Nanoclusters. The $Au_n(SG)_m$ nanoclusters were prepared by a modified literature method.[29] Typically, $HAuCl_4\cdot 3H_2O$ (102 mg, 0.26 mmol) and 1.1 mmol

of H-SG were dissolved in 50 mL of methanol. The solution was then cooled to 0 °C in an ice bath for 30 min. Then, 5 mL of an aqueous solution of $NaBH_4$ (99 mg, 2.6 mmol) was poured rapidly into the mixture under vigorous stirring at 0 °C. The mixture was allowed to react for an additional 2 h. The reaction mixture was centrifuged to remove the insoluble Au(I)-SG polymers. The supernatant was collected and concentrated by rotary evaporation. The concentrated solution was then precipitated by adding acetone. The precipitate was collected and then etched with excess glutathione at 55 °C in water for 3 h. The etched product was then centrifuged to remove insoluble Au(I)-SG polymers as a precipitate. The supernatant was precipitated with ethanol. The precipitate was washed three times with ultrasonication and centrifugation to obtain the clean product. This product was finally run through the polyacrylamide gel electrophoresis (PAGE) gel to obtain pure $Au_{15}(SG)_{13}$, $Au_{18}(SG)_{14}$, $Au_{25}(SG)_{18}$, and $Au_{38}(SG)_{24}$ nanoclusters, which showed up as four distinct bands in gel analysis.

Purification by Polyacrylamide Gel Electrophoresis. The PAGE experiment was conducted by using an OWL P10DS-2 vertical gel electrophoresis system. The gel size was 20 cm × 20 cm. The separating and stacking gels were prepared with monomer (acrylamide) concentrations of 30 and 4%, respectively, with a cross-linker bis-acrylamide concentration of 4% for the best separation. The gel was eluted with 25 mM Tris and 192 mM glycine buffer for 16 h at 300 V. The cluster was dissolved in a 10% (v/v) glycerol/water mixture and loaded in the gel. The well-resolved bands in the gel were cut, crushed, and soaked into water for 2 h. The nanoclusters diffuse into water because of their water solubility. The nanocluster solution with the gel matrix was then filtered with a 0.2 μm filter and then acidified with 100 μL of 10% (v/v) glacial acetic acid. This acidified solution was then concentrated by a cutoff filter of 3 kDa. The concentrated solution was then precipitated with ethanol and dried under vacuum to obtain pure nanoclusters.

To analyze the degradation of the nanoclusters after catalysis, the solutions of pure nanoclusters and the nanoclusters after catalysis were run side by side in the gel and the resultant nanoclusters were isolated from the gel.

Synthesis of $Au_{25}(Capt)_{18}$ Nanoclusters.[30] $HAuCl_4\cdot 3H_2O$ (0.20 mmol, 78.7 mg) and TOABr (0.23 mmol, 126.8 mg) were first dissolved in 10 mL of methanol and vigorously stirred for 15 min. After that, captopril (1 mmol, 217.2 mg) was dissolved in 5 mL of methanol and that solution was rapidly poured into the reaction mixture, and the mixture was stirred for a further 30 min. The color of the solution quickly changed to white. After 30 min, $NaBH_4$ (2 mmol, 75.6 mg) was dissolved in 5 mL of ice-cold water and rapidly added to the solution in the flask under vigorous stirring. The color of the solution immediately changed to brown-black. The reaction was conducted further overnight. Then, the reaction mixture was centrifuged to remove the insoluble Au(I)-Capt polymers. The supernatant was collected and concentrated by rotary evaporation. The concentrated solution was then precipitated by adding acetone. The precipitate was extracted several times with minimal amounts of methanol and then finally precipitated with acetone and dried under vacuum.

Characterization of Gold Nanoclusters. UV−vis spectra of the clusters (dissolved in water) were acquired on a Hewlett-Packard (HP) Agilent 8453 diode array spectrophotometer at room temperature. Matrix-assisted laser desorption ionization
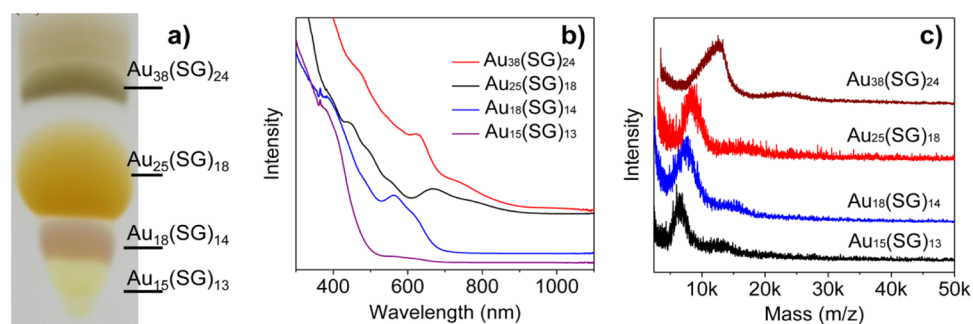
Figure 1. (a) Full gel image of the synthesized $Au_n(SG)_m$ nanoclusters [including $Au_{15}(SG)_{13}$, $Au_{18}(SG)_{14}$, $Au_{25}(SG)_{18}$, and $Au_{38}(SG)_{24}$ nanoclusters and another unidentified nanocluster] after PAGE purification. (b) UV−vis spectra and (c) Matrix-assisted laser desorption ionization mass spectra of the $Au_n(SG)_m$ nanoclusters.

(MALDI) mass spectrometry was performed with a PerSeptiveBiosystems Voyager DE super-STR time-of-flight (TOF) mass spectrometer. 2,4-Dihydroxybenzoic acid (DHB) was used as the matrix during MALDI analysis. The isolated nanoclusters and the matrix were dissolved in a 50% water/methanol mixture to prepare a 1 μM solution (the same concentration for both clusters and DHB). Equal volumes of the matrix and the nanocluster solutions were mixed, and then 5 μL of this mixture was deposited on a MALDI steel plate and dried in a vacumm oven prior to MALDI analysis.

Typical Procedure for the Hydrogenation of Nitrobenzaldehyde. In a typical selective hydrogenation reaction, 4-nitrobenzaldehyde (0.05 mmol), pyridine (0.1 mmol), $Au_n(SG)_m$ nanoclusters (∼0.1 μmol), and 1 mL of water were added to a reactor (Parr Instrument Co., 22 mL capacity, series 4700) under 20 bar of H_2. The reaction mixture was kept at 80 °C. After the reaction, the mixture was extracted with ethyl acetate. The crude product was obtained after the removal of solvent. The conversion of 4-nitrobenzaldehyde and the selectivity for 4-nitrobenzyl alcohol were determined by ^{1}H nuclear magnetic resonance (NMR) (300 MHz) spectroscopic analysis. After the hydrogenation reaction, the gold nanocluster catalyst was analyzed by the UV−vis spectrum and PAGE.

Computational Details. Parallel, resolution-of-identity density functional theory (DFT) calculations with the Perdew−Burke−Ernzerhof form of the generalized gradient approximation for electron exchange and correlation,[31] the def2-SV(P) basis sets, and empirical dispersion correction[32] were performed with the quantum chemistry program Turbomole version 6.5.[33] Effective core potentials that have 19 valence electrons and include scalar relativistic corrections were used for Au.[34] To calculate the surface area of a cluster in a solvent such as water, one constructs a cavity by uniting atom-centered spheres with radii of r_i and r_{solv} for all atoms i in the cluster.[35] Default values for r_i and r_{solv} from Turbomole version 6.5 are used. The surface area of the cavity is defined as the surface area of the cluster.
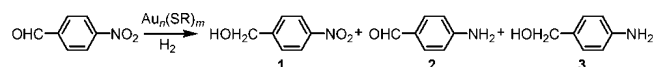
■ RESULTS AND DISCUSSION

The catalytic reactivity of metal nanoclusters mainly depends on the metal core, such as the surface-to-volume ratio, size, morphology, stability, etc.[36−40] Meanwhile, the organic functional shell can affect the electronic properties of the metal core and further influence the catalytic properties of the metal clusters, leading to peculiar selectivity in catalytic reactions. For example, it was found that the catalytic activity of different sized nanoclusters decreases in the following order in the selective

oxidation of styrene: $Au_{25}(SR)_{18} > Au_{38}(SR)_{24} > Au_{144}(SR)_{60}$.[39] Inspired by the results described above, we chose five different aqueous soluble gold nanoclusters protected by functional thiolate ligands, i.e., $Au_{15}(SG)_{13}$, $Au_{18}(SG)_{14}$, $Au_{25}(SG)_{18}$, $Au_{38}(SG)_{24}$, and $Au_{25}(Capt)_{18}$, to investigate the size dependence of the gold nanoclusters and the steric effect of the protecting organic ligands in the chemoselective hydrogenation of the reactants with nitro and aldehyde groups using water as the solvent.

Nanocluster Synthesis and Characterization. The atomically precise $Au_n(SG)_m$ nanoclusters were synthesized by a literature approach[29] but with the following modifications. Briefly, the $Au_n(SG)_m$ nanocluster mixture was first obtained via $NaBH_4$ reduction of $HAuCl_4$ in the presence of excess glutathione. Then the reaction mixture was etched by excess glutathione at 55 °C for 3 h, followed by purification via PAGE. It is worth noting that we modified the previous approach[29] by incorporating the etching step, as this process is very useful for size focusing of the polydispered gold nanoclusters into only several robust sizes. Unlike the reported approach (e.g., the size ranged from Au_{10} to Au_{39}),[29] in our modified synthesis, only $Au_{15}(SG)_{13}$, $Au_{18}(SG)_{14}$, $Au_{25}(SG)_{18}$, and $Au_{38}(SG)_{24}$ nanoclusters were present after size focusing, and they are readily separated by PAGE (Figure 1a). The purified $Au_n(SG)_m$ nanoclusters were characterized by UV−vis spectra (Figure 1b) and matrix-assisted laser desorption ionization (MALDI) mass spectra (Figure 1c) using 2,4-dihydroxybenzoic acid (DHB) as the matrix. $Au_n(SG)_m$ nanoclusters of each size exhibit their characteristic UV−vis spectra with multiple peaks, which can conveniently serve as the fingerprints for the purpose of identification. Their sizes are assigned according to the previous work by comparing the UV−vis spectra with standard spectra.[29] The MADLI mass spectra of $Au_n(SG)_m$ nanoclusters gave rise to broadened peaks due to MALDI-caused ligand loss and other processes, but their peak masses roughly match the expected values. Specifically, $Au_{15}(SG)_{13}$ nanoclusters show saddlelike double peaks at 375/485 nm in the optical spectrum (Figure 1a) and a mass peak centered at m/z ∼6.2k (intact formula mass of 6.9k, where k = 1000) (Figure 1b). In the case of $Au_{18}(SG)_{14}$ nanoclusters, a sharp optical peak at 570 nm and a mass peak centered at m/z ∼6.8k are seen (intact formula mass of 7.8k). The $Au_{25}(SG)_{18}$ nanoclusters give rise to a distinct peak at 670 nm in the UV−vis spectrum and a mass peak at m/z ∼9.4k (intact formula mass of 10.4k). A sharp peak at 630 nm is shown in the UV−vis spectrum of $Au_{38}(SG)_{24}$, and its mass peak is centered at m/z ∼13.6k (intact formula mass of 14.8k). The UV−vis spectra of the four gold nanoclusters [i.e.,

Au$_{15}$(SG)$_{13}$, Au$_{18}$(SG)$_{14}$, Au$_{25}$(SG)$_{18}$, and Au$_{38}$(SG)$_{24}$] match well with the literature.[29] The as-obtained pure Au$_n$(SG)$_m$ nanoclusters are then utilized in catalytic hydrogenation.

Table 1. Hydrogenation of 4-Nitrobenzaldehyde Catalyzed by Unsupported Aqueous Soluble Au$_n$(SG)$_m$ Nanoclusters as Catalysts[a]

OHC—⟨⟩—NO$_2$ $\xrightarrow[\text{H}_2]{\text{Au}_n(\text{SR})_m}$ HOHC$_2$—⟨⟩—NO$_2$ + OHC—⟨⟩—NH$_2$ + HOH$_2$C—⟨⟩—NH$_2$

                         1   **2**   **3**

			selectivity (%)[b]		
entry	catalyst	conversion (%)[b]	1	2	3
1	Au$_{15}$(SG)$_{13}$	7.8	100	nd[d]	nd[d]
2	Au$_{18}$(SG)$_{14}$	10.2	100	nd[d]	nd[d]
3	Au$_{25}$(SG)$_{18}$	16.0	100	nd[d]	nd[d]
4	Au$_{38}$(SG)$_{24}$	20.6	100	nd[d]	nd[d]
5	glutathione	nr[c]	–	–	–

[a]Reaction conditions: 0.1 μmol of unsupported Au$_n$(SG)$_m$ nanocluster catalyst in 1 mL of water, 0.05 mmol of 4-nitrobenzaldehyde (molar ratio of nitrobenzaldehyde to Au clusters of 500), and 0.1 mmol of pyridine under 20 bar of H$_2$ at 80 °C for 4 h. [b]The conversion of 4-nitrobenzaldehyde and selectivity for 4-nitrobenzyl alcohol (**1**) were determined by the ^{1}H NMR spectrum. [c]No reaction. [d]Not detected.

Chemoselective Hydrogenation. Homogeneous hydrogenation was conducted under 20 bar of H$_2$ gas at 80 °C for 4 h in water (for details, see Experimental Methods). After the catalytic reaction, the crude product was analyzed by ^{1}H NMR spectroscopy; only two species, i.e., the residual reactant (4-nitrobenzaldehyde) and only one product [4-nitrobenzyl alcohol (**1**)], are observed in the NMR spectrum (Figure 2).
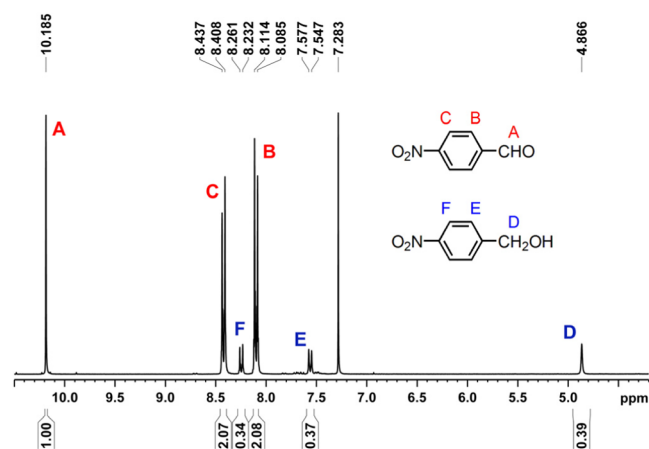

Figure 2. ^{1}H NMR spectrum of the crude product after the catalytic reaction catalyzed by the Au$_{25}$(SG)$_{18}$ nanocluster catalyst. Only residual reactant 4-nitrobenzaldehyde (-C**H**O at 10.18, the proton on the phenyl ring at 8.44 and 8.41, 8.11, and 8.08 ppm) and the exclusive 4-nitrobenzyl alcohol product (-C**H**$_2$ at 4.87, the proton on phenyl ring at 8.26 and 8.23, 7.58, and 7.55 ppm) are found in the spectrum.

Other possible products [e.g., 4-aminobenzaldehyde (**2**) and 4-aminobenzyl alcohol (**3**)] are not detected. As shown in Figure 2, the residual 4-nitrobenzaldehyde shows signals at δ 10.18 (-C**H**O, 1H, s), 8.42 (2H, d), and 8.10 (2H, d), and the chemoselective hydrogenation product (4-nitrobenzyl alcohol) shows signals at δ 8.25 (2H, d), 7.56 (2H, d), and 4.87 ppm (-C**H**$_2$OH, 2H, s). The extra peak at 7.28 ppm belongs to the residual solvent peak of CDCl$_3$. The NMR analysis indicates

that the chemoselectivity for the product of 4-aminobenzyl alcohol is ~100% under the catalysis by the Au$_n$(SG)$_m$ nanocluster catalysts. This complete chemoselectivity is the same as in our previous work involving Au$_n$(SPh)$_m$ nanoclusters,[25] indicating that the surface ligands (SG vs SPh) do not affect the catalytic selectivity (i.e., ~100% in both cases).

Size Dependence of Nanoclusters. With respect to the size dependence of nanoclusters, the conversion of 4-nitrobenzaldehyde when catalyzed by Au$_{15}$(SG)$_{13}$ nanoclusters is relatively low, ~7.8% (Table 1, entry 1). The catalytic activity (hereafter termed the conversion of 4-nitrobenzaldehyde) of the gold nanoclusters increases to 10.2% [Au$_{18}$(SG)$_{14}$], 16.0% [Au$_{25}$(SG)$_{18}$], and 20.6% [Au$_{38}$(SG)$_{24}$] when equal numbers of moles of nanoclusters are used (Table 1, entries 2–4). Thus, the catalytic performance of the gold nanoclusters decreases in the following order: Au$_{38}$(SG)$_{24}$ > Au$_{25}$(SG)$_{18}$ > Au$_{18}$(SG)$_{14}$ > Au$_{15}$(SG)$_{13}$. The observed trend from 7.8 to 20.6% (a nearly 3-fold increase) with increasing cluster size is distinct and interesting. It is worth noting that the selectivity for 4-nitrobenzyl alcohol is constantly 100% in the four hydrogenation reactions described above. No reaction was observed in the blank or control experiments [i.e., using glutathione and captopril ligands as the catalysts under otherwise identical reaction conditions (Table 1, entries 6 and 7, respectively)], indicating that the gold nanoclusters are essential and constitute the catalytically active sites in the hydrogenation reaction. We also note that the catalytic performance of aqueous soluble Au$_{25}$(SG)$_{18}$ is much better than that of the hydrophobic Au$_{25}$(SPh)$_{18}$ catalyst; for instance, the turnover frequency (TOF) of Au$_{25}$(SG)$_{18}$ is ~20 h^{-1} (i.e., moles of alcohol product per hour per mole of gold nanocluster) versus 5.6 h^{-1} [for unsupported Au$_{25}$(SPh)$_{18}$ clusters[25]], which is due to the enhanced activation of H$_2$ in a water solution compared to an organic solution, as evidenced by the higher hydrogenation activity of the gold nanoclusters [e.g., CeO$_2$-supported Au$_{99}$(SPh)$_{42}$ catalyst] in water than in the organic solution (93.1% vs 78.4%).

The Au$_n$(SG)$_m$ nanocluster catalysts [i.e., Au$_{15}$(SG)$_{13}$, Au$_{18}$(SG)$_{14}$, Au$_{25}$(SG)$_{18}$, and Au$_{38}$(SG)$_{24}$], except Au$_{18}$(SG)$_{14}$, are found to be stable and remain intact after the selective hydrogenation, which is supported by the unchanged UV−vis spectra after the hydrogenation reactions (Figure S1 of the Supporting Information). Further analysis of the gold nanocluster catalysts [i.e., Au$_n$(SG)$_m$ after the hydrogenation reactions] by PAGE purification is shown in Figure 3. Only one band appears in the PAGE gel, implying the purity of the nanoclusters. To further confirm the purity of the gel band, we measured the UV−vis spectra at the top and bottom positions of the gel band and found that the Au$_{15}$(SG)$_{13}$, Au$_{25}$(SG)$_{18}$, and Au$_{38}$(SG)$_{24}$ nanoclusters remain intact, judging by the optical spectra being identical to those of the fresh nanoclusters (Figure 3a,c,d vs Figure 1b), while Au$_{18}$(SG)$_{14}$ is less stable and changes to different sized nanoclusters after the catalytic hydrogenation process (Figure 3b vs Figure 1b, blue line).

Ligand Steric Effect. To investigate the potential steric effect of the protecting thiolate ligand, we further chose the captopril-protected Au$_{25}$(Capt)$_{18}$ nanocluster and compared its performance with that of Au$_{25}$(SG)$_{18}$. The captopril ligand is less bulky than glutathione (Scheme 1a). The synthesis of the Au$_{25}$(Capt)$_{18}$ nanocluster follows a reported protocol[30] (see Experimental Methods). The as-obtained Au$_{25}$(Capt)$_{18}$ nanocluster shows a UV−vis spectrum (Figure 4a) identical to that of Au$_{25}$(SG)$_{18}$; note that the slight change in the UV region is
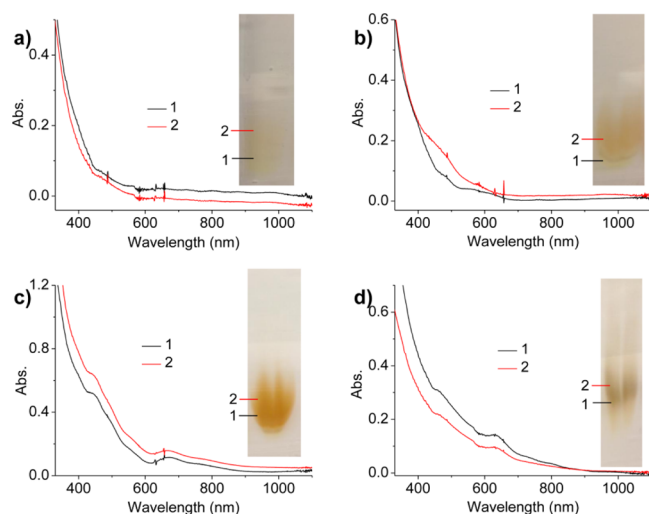
Figure 3. (a−d) Gel images and corresponding UV−vis spectra (at different positions of the gel) of the gold nanocluster catalysts after the hydrogenation: (a) $Au_{15}(SG)_{13}$, (b) $Au_{18}(SG)_{14}$, (c) $Au_{25}(SG)_{18}$, and (d) $Au_{38}(SG)_{24}$.

Table 2. Hydrogenation of 4-Nitrobenzaldehyde Catalyzed by Unsupported Aqueous Soluble $Au_{25}(SR)_{18}$ (SR = SG or Capt) Nanoclusters and the Polymeric Au(I)-SG Complex[a]

entry	catalyst	conversion (%)[b]	selectivity (%)[b]		
			1	2	3
1	$Au_{25}(Capt)_{18}$	23.3	100	nd[d]	nd[d]
2	$Au_{25}(SG)_{18}$	16.0	100	nd[d]	nd[d]
3	Au(I)-SG	65.6	24	76	nd[d]
4	captopril	nr[c]	–	–	–

[a]Reaction conditions: 0.1 μmol of unsupported $Au_{25}(SR)_{18}$ nanocluster or Au(I)-SG complex catalyst in 1 mL of water, 0.05 mmol of 4-nitrobenzaldehyde, and 0.1 mmol of pyridine under 20 bar a H_2 at 80 °C for 4 h. [b]The conversion of 4-nitrobenzaldehyde and selectivity for 4-nitrobenzyl alcohol (**1**) and 4-aminobenzaldehyde (**2**) were determined by the ^{1}H NMR spectrum. [c]No reaction. [d]Not detected.

caused by the trace organic residues (e.g., pyridine and the catalytic product). MALDI mass spectra show a sharp peak around 8.4 kDa (Figure 4b), in which some ligands are lost due to MALDI process (intact mass of 8.8k). The hydrogenation reaction catalyzed by $Au_{25}(Capt)_{18}$ nanoclusters was conducted under conditions identical to those of the $Au_n(SG)_m$ cases. A high conversion [23.3% (Table 2, entry 1)] of 4-nitrobenzaldehyde with 100% selectivity for the 4-nitrobenzyl alcohol product was obtained, which is indeed better than those of the other four glutathione-protected $Au_n(SG)_m$ nanoclusters. The TOF value of the $Au_{25}(Capt)_{18}$ catalyst was increased to ∼30 h^{-1}. The UV−vis spectra and the MALDI mass spectra (Figure 4) indicate that the $Au_{25}(Capt)_{18}$ nanocluster catalyst is intact after the hydrogenation reaction. The higher catalytic activity of the $Au_{25}(Capt)_{18}$ nanocluster catalyst can be attributed to the steric effect [i.e., less bulky captopril compared to the -SG ligand on the surface of the $Au_n(SG)_m$ nanoclusters]. We also found that the Au(I)-SG complex can catalyze the reaction (Figure S2 of the Supporting Information) but the ligand itself cannot. The Au(I)-SG complex gave rise to a 65.6% conversion and a 76% selectivity for the 4-aminobenzaldehyde product and 24% for 4-nitrobenzyl alcohol (Table 2, entry 3).

Further, the selective hydrogenation kinetics was investigated by monitoring the conversion of 4-nitrobenzaldehyde using $Au_{25}(Capt)_{18}$ as a catalyst at different time intervals. To rule out
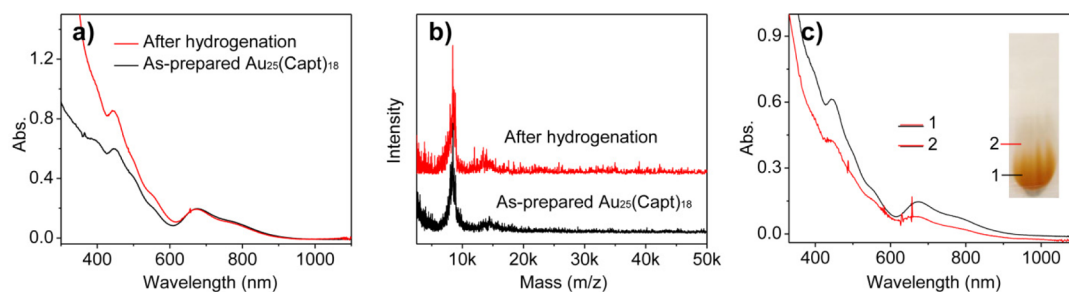
the possibility that the high selectivity (∼100%) might be due to the relatively low conversion in the reaction, we adjusted the reaction conditions to improve the conversion by increasing the amount of $Au_{25}(Capt)_{18}$ catalyst from 0.1 to 0.2 μmol and decreasing the amount of nitrobenzaldehyde from 0.05 to 0.025 mmol (with other reaction conditions kept the same as described in footnote a of Table 1). Under such conditions, the conversion was largely increased to 76.9% at 4 h and 83.2% at 9 h (Figure 5), whereas the chemoselectivity for the alcohol
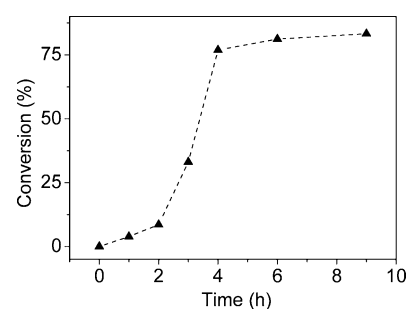

Figure 5. Time-dependent conversion of 4-nitrobenzaldehyde as a function of reaction time over unsupported $Au_{25}(Capt)_{18}$. Reaction conditions: 0.2 μmol of $Au_{25}(Capt)_{18}$ nanocluster catalyst in 2 mL of water, 0.025 mmol of 4-nitrobenzaldehyde, and 0.1 mmol of pyridine under 20 bar of H_2 at 80 °C for 9 h.

product is constantly at ∼100%. Thus, the high chemoselectivity is not due to the relatively low conversion in the reaction; instead, it is the intrinsic characteristics of the catalyst. It is worth noting that the $Au_{25}(Capt)_{18}$ catalyst still remains intact after the catalytic reactions.

Figure 4. (a) UV−vis and (b) MALDI mass spectrometry spectra of the $Au_{25}(Capt)_{18}$ nanocluster catalyst before and after the hydrogenation reaction. (c) Gel images and corresponding UV−vis spectra (at different positions) of the gold nanocluster catalysts after the hydrogenation.

Structure–Property Correlation. $Au_{25}(SCH_2CH_2Ph)_{18}$ and $Au_{38}(SCH_2CH_2Ph)_{24}$ nanoclusters have been crystallographically characterized previously,[13,14] and the $Au_{15}(SCH_3)_{13}$ and $Au_{18}(SCH_3)_{14}$ structures have been predicted by DFT calculation.[27,28] Thus, we chose these four cluster structures as models for the DFT simulations on the 4-nitrobenzaldehyde adsorption mode and further correlated the catalytic activity with the cluster structures. It is worth noting that the capping thiolate ligand (-SG) was replaced by -SCH$_3$ only for the ease of DFT calculations. Calculations from dispersion-corrected DFT suggest that the adsorption energies of the 4-nitrobenzaldehyde ($4\text{-}NO_2PhCHO$) molecule on the four $Au_n(SCH_3)_m$ nanoclusters are moderately strong and similar. The 4-nitrobenzaldehyde molecule has the strongest adsorption on the $Au_{25}(SCH_3)_{18}$ nanoclusters, probably because of the extra negative charge on the native $Au_{25}(SCH_3)_{18}^-$ cluster[13] that provides higher polarizability to a strongly polar group such as -NO$_2$ on the molecule. Figure 6 shows an adsorption
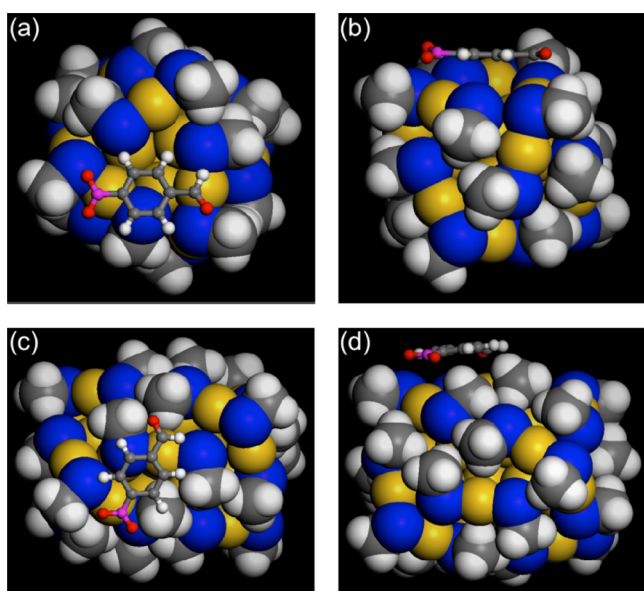

Figure 6. 4-Nitrobenzaldehyde molecule adsorbed on a $Au_{25}(SCH_3)_{18}^-$ nanocluster [top view (a) and side view (b)]. $Au_{38}(SCH_3)_{24}$ nanocluster [top view (c) and side view (d)]. The color code is as follows: yellow for Au, blue for S, gray for C, white for H, red for O, and pink for N.

geometry of the 4-nitrobenzaldehyde molecule on $Au_{25}(SCH_3)_{18}^-$ and $Au_{38}(SCH_3)_{24}$. One can see that the -CHO and -NO$_2$ groups of the molecule are in close contact with the S-Au-S groups of the cluster surface; this interaction is mostly likely due to the polar organic groups inducing dipoles in the S-Au-S motifs. In addition, there are multiple sites on each of the clusters that can adsorb the molecule. The variation in adsorption energy is not large, as indicated by the small difference between the maximal adsorption energy and the average adsorption energy (Table 3); the energy difference is only 0.02 eV for $Au_{18}(SCH_3)_{14}$, $Au_{25}(SCH_3)_{18}$, and $Au_{38}(SCH_3)_{24}$ nanoclusters and 0.11 eV for $Au_{15}(SCH_3)_{13}$. The fact that the Au nanoclusters have multiple sites with similar adsorption energies suggests that the catalytic conversion of the 4-nitrobenzaldehyde molecule on a cluster should correlate with the surface area of the Au nanocluster. We therefore plotted the conversion of the 4-nitrobenzalde-

Table 3. Adsorption Energy of the 4-Nitrobenzaldehyde Molecule on Various $Au_n(SCH_3)_m$ Nanoclusters[a]

entry	Au nanocluster	$E_{\text{ad-max}}$ (eV)	$E_{\text{ad-average}}$ (eV)
1	$Au_{15}(SCH_3)_{13}$	−0.99	−0.88
2	$Au_{18}(SCH_3)_{14}$	−0.94	−0.92
3	$Au_{25}(SCH_3)_{18}$	−1.05	−1.03
4	$Au_{38}(SCH_3)_{24}$	−0.86	−0.86

[a]Both the adsorption energy for the maximal interaction ($E_{\text{ad-max}}$) and the average interaction over several adsorption sites ($E_{\text{ad-average}}$) are listed. They were computed at the dispersion-corrected DFT-PBE level (DFT-PBE-D3) with the def2-SV(P) basis sets in Turbomole. A negative value means a favorable interaction.

hyde molecule on the basis of the same number of moles of the $Au_n(SCH_3)_m$ nanoclusters against the surface area of the cluster (Figure 7) and found that indeed the conversion increases with the surface area of the gold cluster (see Computational Details for how the surface area is calculated).
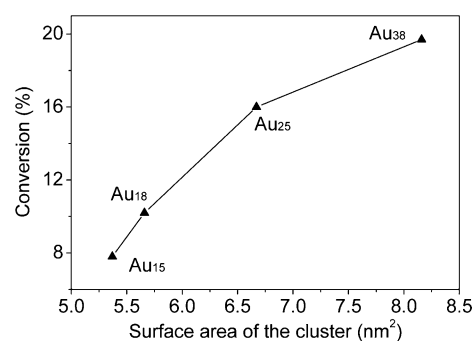

Figure 7. Conversion of 4-nitrobenzaldehyde vs the surface area of the $Au_n(SCH_3)_m$ nanoclusters.

On the basis of the experimental results discussed above and DFT simulations, here we briefly discuss the plausible mechanism for selective hydrogenation. The 4-nitrobenzaldehyde ($4\text{-}NO_2PhCHO$) molecules are first adsorbed onto the $Au_x(SR)_{x+1}$ staples of the $Au_n(SR)_m$ nanocluster; both the -NO$_2$ and -CHO groups strongly interact with the S-Au-S staple motifs on the cluster surface. At the same time, H$_2$ is activated by the gold nanoclusters under the assistance of pyridine. Then the -CHO group is selectively hydrogenated via the surface Au atoms. Finally, the 4-nitrobenzyl alcohol molecule is formed and desorbed from the Au nanocluster catalyst.

CONCLUSIONS

In summary, we have investigated the catalytic properties of water-soluble $Au_n(SR)_m$ nanocluster catalysts [including $Au_{15}(SG)_{13}$, $Au_{18}(SG)_{14}$, $Au_{25}(SG)_{18}$, $Au_{38}(SG)_{24}$, and $Au_{25}(Capt)_{18}$] in the homogeneous chemoselective hydrogenation of 4-nitrobenzaldehyde in water. The well-defined $Au_n(SR)_m$ nanocluster catalysts are essentially intact after the chemoselective hydrogenation, except for the $Au_{18}(SG)_{14}$ nanocluster. Overall, a drastic size dependence and the ligand's steric effects are observed in gold nanocluster-catalyzed hydrogenation reactions. The catalytic activity (based on the conversion of 4-nitrobenzaldehyde) of the gold nanoclusters increases with an increasing core size: $Au_{15}(SG)_{13} < Au_{18}(SG)_{14} < Au_{25}(SG)_{18} < Au_{38}(SG)_{24}$. On the other hand, the catalytic properties of the gold nanoclusters with the less bulky ligand are found to be much better [e.g., $Au_{25}(Capt)_{18} > Au_{25}(SG)_{18}$].

DFT calculations show that both -CHO and -NO$_2$ groups of the 4-nitrobenzaldehyde molecule closely interact with the cluster surface staples (S-Au-S); the adsorption energies of the 4-nitrobenzaldehyde molecule on the four different sized Au$_n$(SR)$_m$ nanoclusters are moderately strong (−0.86 to −1.05 eV). The increased catalytic activity of larger gold nanoclusters is consistent with the surface area of the gold nanoclusters. Overall, this work reveals the molecular level insight into the hydrogenation reaction of nitrobenzaldehyde and the catalytically active site structure on gold nanocluster catalysts.

■ ASSOCIATED CONTENT

Ⓢ Supporting Information

UV−vis spectra of the Au$_n$(SG)$_m$ nanocluster catalysts before and after hydrogenation, and NMR spectrum of the reaction product when catalyzed by the Au(I):SG polymer. This material is available free of charge via the Internet at http://pubs.acs.org.

■ AUTHOR INFORMATION

Corresponding Author
*E-mail: rongchao@andrew.cmu.edu.

Notes
The authors declare no competing financial interest.

■ ACKNOWLEDGMENTS

■ REFERENCES

(1) Yamazoe, S.; Koyasu, K.; Tsukuda, T. Acc. Chem. Res. 2014, 47, 816−824.
(2) Qian, H.; Zhu, M.; Wu, Z.; Jin, R. Acc. Chem. Res. 2012, 45, 1470−1479.
(3) Yu, Y.; Luo, Z.; Chevrier, D. M.; Leong, D. T.; Zhang, P.; Jiang, D.; Xie, J. J. Am. Chem. Soc. 2014, 136, 1246−1249.
(4) Yi, C.; Tofanelli, M. A.; Ackerson, C. J.; Knappenberger, K. L., Jr. J. Am. Chem. Soc. 2013, 135, 18222−18228.
(5) Kwak, K.; Kumar, S. S.; Pyo, K.; Lee, D. ACS Nano 2014, 8, 671−679.
(6) Mathew, A.; Natarajan, G.; Lehtovaara, L.; Häkkinen, H.; Kumar, R. M.; Subramanian, V.; Jaleel, A.; Pradeep, T. ACS Nano 2014, 8, 139−152.
(7) Kwak, K.; Kumar, S. S.; Lee, D. Nanoscale 2012, 4, 4240−4246.
(8) Sakai, N.; Tatsuma, T. Adv. Mater. 2010, 22, 3185−3188.
(9) Li, G.; Jin, R. Acc. Chem. Res. 2013, 46, 1749−1758.
(10) Li, G.; Jiang, D.; Liu, C.; Yu, C.; Jin, R. J. Catal. 2013, 306, 177−183.
(11) Li, G.; Liu, C.; Lei, Y.; Jin, R. Chem. Commun. 2012, 48, 12005−12007.
(12) Liu, J.; Krishna, K. S.; Losovyj, Y. B.; Chattopadhyay, S.; Lozova, N.; Miller, J. T.; Spivey, J. J.; Kumar, C. Chem.—Eur. J. 2013, 19, 10201−10208.
(13) Zhu, M.; Aikens, C. M.; Hollander, F. J.; Schatz, G. C.; Jin, R. J. Am. Chem. Soc. 2008, 130, 5883−5885.
(14) Qian, H.; Eckenhoff, W. T.; Zhu, Y.; Pintauer, T.; Jin, R. J. Am. Chem. Soc. 2010, 132, 8280−8281.
(15) Mitsudome, T.; Kaneda, K. Green Chem. 2013, 15, 2636−2654.
(16) Pan, M.; Brush, A. J.; Pozun, Z. D.; Ham, H. C.; Yu, W.; Henkelman, G.; Hwang, G. S.; Mullins, C. B. Chem. Soc. Rev. 2013, 42, 5002−5013.
(17) Yamane, Y.; Liu, X.; Hamasaki, A.; Ishida, T.; Haruta, M.; Yokoyama, T.; Tokunaga, M. Org. Lett. 2009, 11, 5162−5165.
(18) Corma, A.; Serna, P. Science 2006, 313, 332−334.
(19) Cano, I.; Chapman, A. M.; Urakawa, A.; van Leeuwen, M. J. Am. Chem. Soc. 2014, 136, 2520−2528.
(20) Ren, D.; He, L.; Yu, L.; Ding, R.; Liu, Y.; Cao, Y.; He, H.; Fan, K. J. Am. Chem. Soc. 2012, 134, 17592−17598.
(21) Santos, L. L.; Serna, P.; Corma, A. Chem.—Eur. J. 2009, 15, 8196−8203.
(22) Zhu, Y.; Qian, H.; Drake, B. A.; Jin, R. Angew. Chem., Int. Ed. 2010, 49, 1295−1298.
(23) Yamamoto, H.; Yano, H.; Kouchi, H.; Obora, Y.; Arakawa, R.; Kawasaki, H. Nanoscale 2012, 4, 4148−4154.
(24) Shivhare, A.; Ambrose, S. J.; Zhang, H.; Purves, R. W.; Scot, R. W. J. Chem. Commun. 2013, 49, 276−278.
(25) Li, G.; Zeng, C.; Jin, R. J. Am. Chem. Soc. 2014, 136, 3673−3679.
(26) Zhu, Y.; Wu, Z.; Gayathri, G. C.; Qian, H.; Gil, R. R.; Jin, R. J. Catal. 2010, 271, 155−160.
(27) Jiang, D.; Overbury, S. H.; Dai, S. J. Am. Chem. Soc. 2013, 135, 8786−8789.
(28) Tlahuice, A.; Garzón, I. L. Phys. Chem. Chem. Phys. 2012, 14, 3737−3740.
(29) Negishi, Y.; Nobusada, K.; Tsukuda, T. J. Am. Chem. Soc. 2005, 127, 5261−5270.
(30) Kumar, S.; Jin, R. Nanoscale 2012, 4, 4222−4227.
(31) Perdew, J. P.; Burke, K.; Ernzerhof, M. Phys. Rev. Lett. 1996, 77, 3865−3868.
(32) Grimme, S.; Antony, J.; Ehrlich, S.; Krieg, H. J. Chem. Phys. 2010, 132, 154104.
(33) Ahlrichs, R.; Bar, M.; Haser, M.; Horn, H.; Kolmel, C. Chem. Phys. Lett. 1989, 162, 165−169.
(34) Andrae, D.; Haussermann, U.; Dolg, M.; Stoll, H.; Preuss, H. Theor. Chim. Acta 1990, 77, 123−141.
(35) Klamt, A. WIREs Computational Molecular Science 2011, 1, 699−709.
(36) Haruta, M. Catal. Today 1997, 36, 153−166.
(37) Fenger, R.; Fertitta, E.; Kirmse, H.; Thünemann, A. F.; Rademann, K. Phys. Chem. Chem. Phys. 2012, 14, 9343−9349.
(38) Nikolaev, S. A.; Smirnov, V. V. Catal. Today 2009, 147, S336−S341.
(39) Zhu, Y.; Qian, H.; Jin, R. Chem.—Eur. J. 2010, 16, 11455−11462.
(40) Liu, Y.; Tsunoyama, H.; Akita, T.; Xie, S.; Tsukuda, T. ACS Catal. 2011, 1, 2−6.